



Influence of droplet transfer behaviour on the microstructure, mechanical properties and corrosion resistance of wire arc additively manufactured Inconel (IN) 625 components

Rama Kishore Mookara¹ · Saravanan Seman^{1,2} · R. Jayaganthan² · Murugaiyan Amirthalingam¹

Received: 26 October 2020 / Accepted: 27 November 2020 / Published online: 5 January 2021
© International Institute of Welding 2021

Abstract

A Ni-based superalloy, Inconel 625, is widely used for aerospace, petrochemical and marine applications due to its excellent corrosion and elevated temperature mechanical properties. In this study, efforts were made to identify optimum deposition parameters to produce directionally solidified Inconel 625 components using wire arc additive manufacturing (WAAM). Components were deposited by short-circuiting and short-circuiting with pulse mode of droplet transfers using a commercial cold metal transfer gas metal arc welding (CMT-GMAW) power source. For a given arc energy, metal droplet transfer behaviour was studied using a high-speed camera. Microstructural analysis and corrosion resistance of Inconel 625 samples produced by WAAM and samples made by conventional casting process were compared by advanced characterisation methods. Inconel 625 samples produced using a combination of short-circuiting with pulsing free flight transfers showed improved mechanical properties than as-cast samples and samples made only by short-circuiting transfer due to the formation of directionally solidified coarse-grained columnar microstructure. Moreover, corrosion resistance of WAAM samples was found to be better than that of as-cast samples. Based on the results, an optimised current-voltage waveform and droplet transfer modes were identified to produce defect-free Inconel 625 deposits with desired microstructure, and mechanical and corrosion-resistance properties.

Keywords Wire arc additive manufacturing · Waveform controlled welding · Metal transfer

1 Introduction

In additive manufacturing (AM), also known as additive layer manufacturing (ALM), metallic components are built by adding feedstock sequentially layer by layer. The melting of feedstock materials such as powder or wire can be achieved by using a laser, an electron beam or a welding arc as a heat source [1]. Additive manufacturing using a welding arc as a heat source is commonly known as wire arc additive

manufacturing (WAAM) in which parts are built using a conventional welding setup. High deposition rates and increased process efficiency as compared to other AM processes make WAAM an attractive process to build near net shape large-volume components [2]. WAAM is typically carried out by suitably modifying a gas tungsten arc welding (GTAW) process with filler addition or using gas metal arc welding (GMAW) processes. Cold metal transfer (CMT) process is a variant of GMAW, which is known for giving a negligible amount of spatter during weld deposition with lower heat input and excellent control over microstructural evolution [3]. Due to these advantages, the adaptation of CMT for WAAM has been extensively explored [3, 4].

The Ni-based superalloy Inconel 625 is widely used in aerospace, chemical, petrochemical and marine industries. It has a good combination of yield, tensile, creep strengths, hot ductility, weldability and good resistance to high-temperature corrosion during prolonged exposure to aggressive environments [5]. This combination of properties is due to the solid-solution hardening

Recommended for publication by Commission XII - Arc Welding Processes and Production Systems

✉ Murugaiyan Amirthalingam
murugaiyan@iitm.ac.in

¹ Department of Metallurgical and Materials Engineering, Indian Institute of Technology (IIT) Madras, Chennai, TN, India

² Department of Engineering Design, Indian Institute of Technology (IIT) Madras, Chennai, TN, India

resulting from the addition of refractory metals such as niobium and molybdenum in a nickel-chromium matrix [6]. Inconel 625 components are widely produced in industrial scale by casting, powder metallurgy or forging [7]. Although these methods are capable of producing components for demanding engineering applications, high production costs and quick realisation of complex geometries are recognised as the limiting factors for various critical engineering applications. In general, AM is seen as a feasible and economical alternative to conventional manufacturing methods.

Direct metal deposition (DMD)-based AM processes for producing Inconel 625 components have attracted considerable attention in recent years [8]. Attempts were also made to deposit Inconel 625 alloy by pulsed plasma arc deposition [9], gas tungsten arc welding [10, 11] and cold metal transfer (CMT)-based welding processes [12, 13].

There were attempts made to study the corrosion behaviour of Inconel 625 components produced by laser powder bed fusion and wire arc additive manufacturing processes. Cabrini *et al.* evaluated the corrosion resistance of Inconel 625 produced by laser powder bed fusion and compared with samples made through conventional casting and hot working route [14]. Wang *et al.* investigated the microstructure and corrosion properties of Inconel 625 alloy fabricated by the CMT-GMAW-based WAAM process [15]. It was also shown that the presence of Laves and other intermetallic phases in the Inconel 625 deposit accelerated the localised corrosion rate and pitting corrosion under high-temperature and high-pressure (HTHP) H_2S/CO_2 conditions [16]. The corrosion behaviour of Inconel 625 is known to get affected by the grain structure, grain morphology, and presence of detrimental intermetallic phases. There are no attempts so far made to control the evolution of microstructure favourably by using suitable current-voltage waveforms and metal droplet transfer behaviour during WAAM of Inconel 625 components. Therefore, an attempt is made in this work to stabilise the microstructural constituents required to achieve good corrosion and mechanical properties in Inconel 625 samples deposited by WAAM.

In this work, Inconel 625 alloy components were deposited by the CMT-GMAW-based WAAM process. Depositions were made by short-circuiting and short-circuiting with pulse mode of droplet transfer using a commercial cold metal transfer gas metal arc welding (CMT-GMAW) power source. The process stability was evaluated by observing droplet transfer behaviour for a given arc energy using a high-speed camera. Microstructural characterisation was carried out on the Inconel 625 deposits by optical (OM) and scanning electron microscopy (SEM). Tensile properties were studied along the longitudinal and normal sections of deposits, and the resultant fracture surfaces were analysed.

The electrochemical corrosion behaviour of the WAAM samples were compared with conventionally manufactured as-cast Inconel 625 alloy samples. Results showed that deposition made using a combination of controlled dip short-circuiting with pulsing free flight metal transfer is suitable to fabricate defect-free deposits with desired microstructural, mechanical and corrosion properties.

2 Materials and methods

2.1 Material deposition

The experimental setup used for WAAM was the same as reported by the authors in their earlier work [3]. The CMT-GMAW torch was mounted along the normal direction on a computerised numerical control (CNC) table. Using a PLC-based G-code program, movement of the torch was controlled along the specified build path in three directions. Mild steel with a size of $150 \times 70 \times 3 \text{ mm}^3$ was used as substrate, and it was clamped on a stainless steel base plate. A commercial Inconel 625 filler wire (ERNicrMo-3) of 1.2 mm diameter was used as a feedstock. The chemical composition of filler and substrate is provided in Table 1. Prior to the deposition, the substrate was ground with a 320 grit SiC paper and degreased with acetone. Depositions were made on the substrate using argon shielding gas (99.999% purity) using a Fronius-TranspulsTM synergic 4000 CMT welding power source in short-circuiting and short-circuiting with pulse mode of droplet transfers with optimised parameters given in Table 2.

Samples manufactured using the short-circuiting mode of droplet transfer consisted of 13 layers with a total height 50 mm and width of 12 mm while samples manufactured with short-circuiting with pulse mode of droplet transfer consisted of 13 layers with a total height of 60 mm and width of 20 mm (Fig. 1). Samples produced by WAAM were compared with samples extracted from a commercial centrifugally cast Inconel 625 pipe (Fig. 1d). During the multi-pass deposition, it was ensured that the previously deposited layer was completely cooled to room temperature. Before the onset of next deposition, the previously deposited layer was cleaned with a stainless steel wire brush.

An InfiniVisionTM digital storage oscilloscope was used to record the current and voltage waveforms during the deposition with a recording frequency of 70 kHz. A Photon FASTCAM high-speed camera was used to observe melt pool stability and droplet transfer behaviour during the multi-pass deposition. The imaging rate of the high-speed CCD camera was 6000 frames per second with an image resolution of 896×752 pixels.

The arc energy during each deposition was calculated using [17]

Table 1 Chemical composition of Inconel 625 filler wire and cast Inconel 625 alloy

Inconel 625 filler	Alloying additions in filler wire (wt%)											
	Ni	C	Mn	Fe	Si	Al	Ti	Cr	Nb + TA	Mo	S	P
	64	0.011	< 0.0001	0.17	0.12	0.13	0.21	22.4	3.59	8.8	–	–
Inconel 625 cast pipe	Alloying additions in Inconel 625 cast pipe (wt%)											
	64	0.06	0.50	5.0	1.00	0.40	0.40	21.5	3.65	9	–	–
Mild steel substrate	Alloying elements in mild steel (wt%)											
	–	0.28	1.03	Balance	0.280	–	–	–	–	–	–	0.05

$$IP = \frac{1}{n} \sum_{i=0}^n (I_i \cdot U_i) \quad (1)$$

where IP is instantaneous power (W), I_i is instantaneous current (A) and U_i is instantaneous voltage (V).

$$\text{Arc energy} = \frac{IP \cdot \eta}{v} \quad (2)$$

where v is welding speed (400 mm min^{-1}) and η is process efficiency. For ease of calculations, η is assumed to be 1 and the calculated arc energy is given in Table 2.

2.2 Microstructural and mechanical characterisation

Samples were extracted using an electro discharge machine (EDM) along the transverse direction (X - Z plane) of WAAM deposits and as-cast alloy for metallography analysis. The metallographically polished Inconel 625 alloy samples were etched using Kalling's reagent (100 ml of hydrochloric acid, 100 ml of ethanol and 5 grams of CuCl_2). Microstructural analysis was carried out using an Olympus inverted light microscope and Inspect F field emission gun scanning electron microscope (FE-SEM) equipped with an energy-dispersive spectroscope (EDS). Vickers hardness measurement was carried out along the transversal direction (X - Z plane) from the substrate to top layers using a 300-g load. For tensile tests, samples were extracted along the transversal (X - Z plane) and longitudinal (Y - Z plane) directions of WAAM deposits (Fig. 2a). Tensile

samples from as-cast Inconel alloy were machined along the longitudinal (length, Y) direction in X - Z and Y - Z planes. Tensile tests were carried out with a strain rate of 10^{-3} s^{-1} using sub-sized flat specimens with 1.5 mm thickness, 10 mm gauge length, 3 mm gauge width and 40 mm overall length as per ASTM E8 standard (Fig. 2b). Subsequently, the fracture surfaces were analysed by scanning electron microscopy.

2.3 Corrosion analysis

The electrochemical experiments for corrosion analysis were carried out on WAAM and as-cast Inconel 625 alloy samples. Samples with a dimension of $15 \times 15 \times 4 \text{ mm}^3$ were extracted at three locations covering four layers from the deposits, at the bottom (BL), middle (ML) and top (TL), as shown in Fig. 3. Samples were ground and polished with 300 to 2400 grit SiC emery papers. Subsequently, all the specimens were ultrasonically cleaned in acetone and dried with a stream of hot air. Electrochemical experiments were performed in 350 ml, 0.1 M NaCl solution with an exposed area of 0.785 cm^2 . Potentiodynamic polarisation and electrochemical impedance spectroscopy (EIS) analyses were made using WAAM and as-cast samples as working electrodes, a saturated calomel electrode as the reference and a platinum wire as a counter electrode. All samples were subjected to an open-circuit potential (OCP) test for 1 h before conducting EIS and potentiodynamic polarisation studies. EIS measurements were performed at OCP with an impedance range of 100,000 Hz to 0.01 Hz. The potentiodynamic polarisation tests were carried out from -300 to 900 mV versus E_{ocp} at a scan rate of 0.1667 mV s^{-1} .

Table 2 Deposition parameters

List of parameters	Mode of droplet transfer	
	Short-circuiting	Short-circuiting with pulse
Set current (A)	115	85
Voltage (V)	9.95	10.4
Travel speed (mm min^{-1})	400	400
Contact tip to workpiece distance (mm)	15	15
Wire diameter (mm)	1.2	1.2
Arc energy (J mm^{-1})	172	176

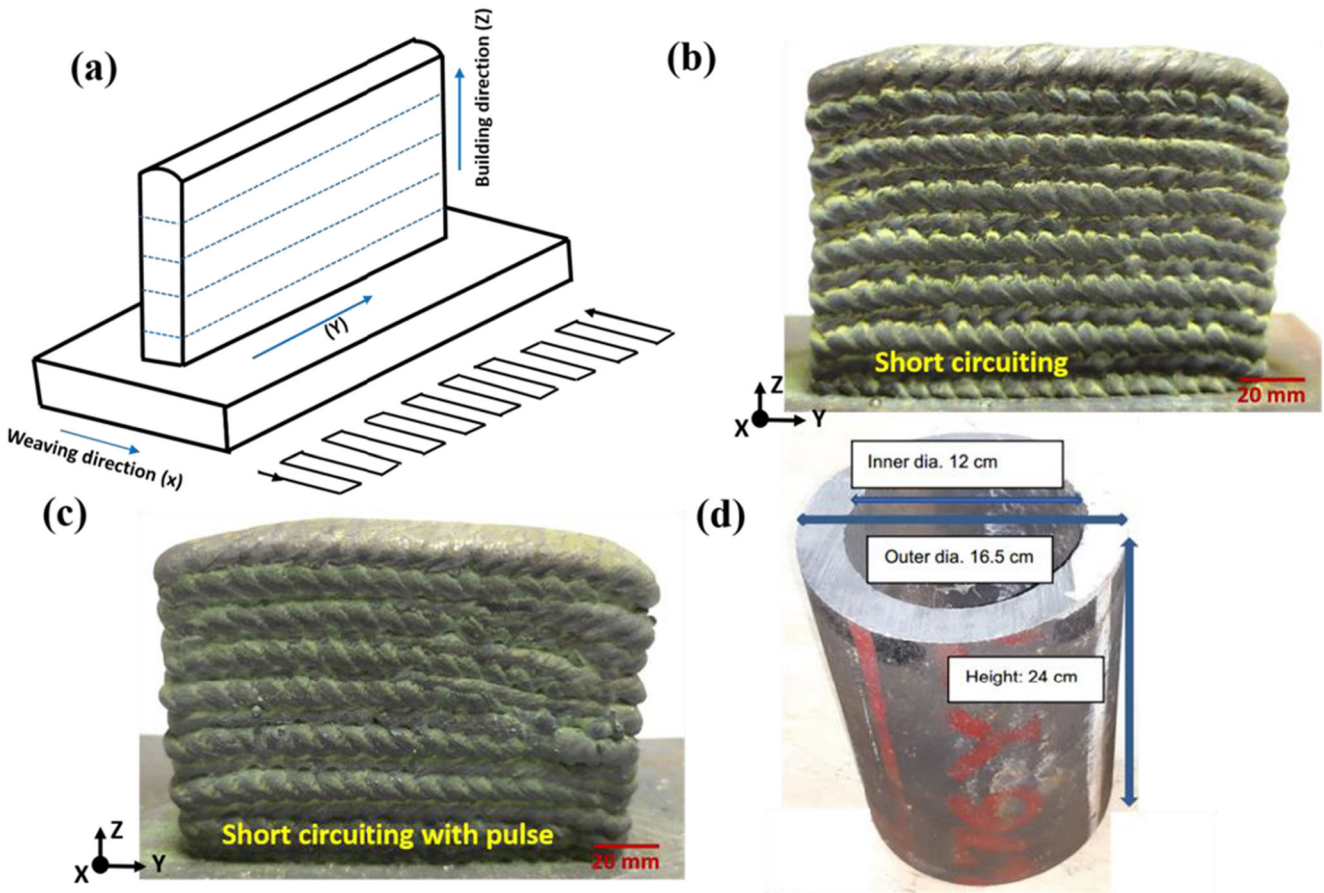


Fig. 1 Schematic representation of the WAAM deposition process of Inconel 625 (a), samples fabricated by CMT-WAAM with the short-circuiting mode of droplet transfer (b), deposited with short-circuiting with pulse mode of droplet transfer (c), and conventionally cast pipe (d)

All the electrochemical experiments were carried out at 25 °C according to ASTM F-2129 standard, and the corrosion rate was calculated as per ASTM G-102. The data obtained were analysed using the software GAMRY Echem analyst version 7.06.

The corrosion rate was calculated by using [18]

$$\text{corrosion rate} = \frac{k.W.I}{\rho.A} \tag{3}$$

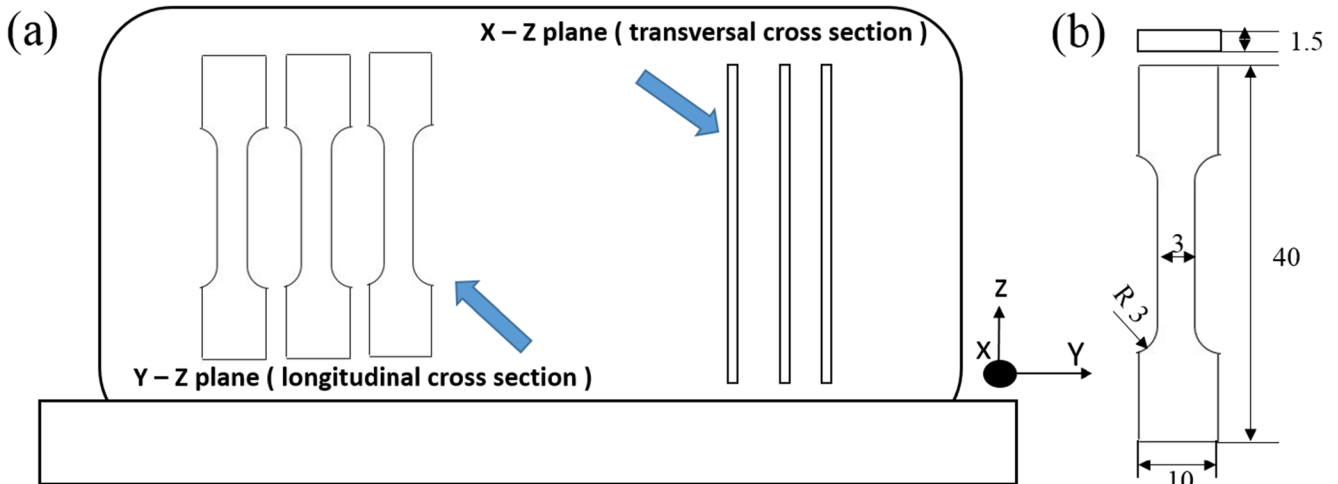


Fig. 2 Schematic representation of positions from which tensile specimens were extracted (a) and ASTM E8 sub-sized tensile specimen dimensions in mm (b)

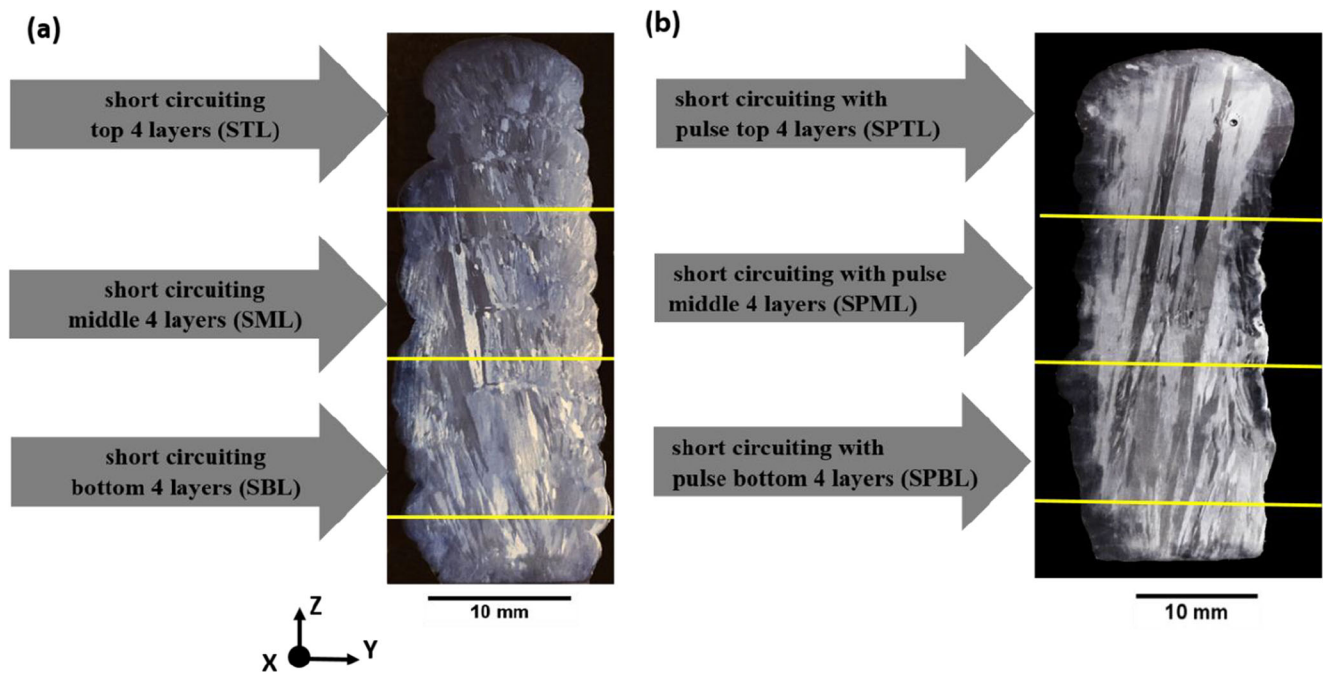


Fig. 3 Schematic representation of the positions from which corrosion testing samples were extracted. From the bottom, middle, and top layers of deposits made by short-circuiting, SBL, SML, and STL, respectively

where k is the corrosion constant in mills per year (MPY), W is equivalent weight, I is current, ρ is density and A is the cross-sectional area of the sample.

3 Results

3.1 Process stability under short-circuiting and short-circuiting with pulse deposition of Inconel 625 filler

Inconel 625 alloy filler was deposited under short-circuiting and short-circuiting with pulse mode to identify suitable process and metal droplet transfer characteristics. Figure 4 shows the metal transfer characteristics of Inconel 625 filler under

(a), and short-circuiting with pulse, SPBL, SPML, and SPTL, respectively (b)

short-circuiting transfer mode. The duration between two short-circuiting processes was 12.5 ms. Arc was ignited at 0 ms and, subsequently, the current was increased up to 300 A. At this peak current (I_p), the filler wire was molten and droplet was formed at the tip of the electrode at 3.5 ms. At 4.5 ms, the wire moved towards the weld pool and created a short-circuiting event at 6 ms. A droplet was detached to the weld pool at 7 ms followed by the arc re-ignition for the subsequent cycle. Arc energy during this deposition was 172 J mm^{-1} for an instantaneous current (I_i) of 115 A.

Figure 5 shows droplet transfer characteristics of Inconel 625 filler while depositing in short circuiting with pulse mode. Deposition consisted of 22 pulse and a short-circuiting event in a single cycle. The total duration of one cycle (arc ignition to arc re-ignition) was 387 ms. The cycle started at 86 ms with

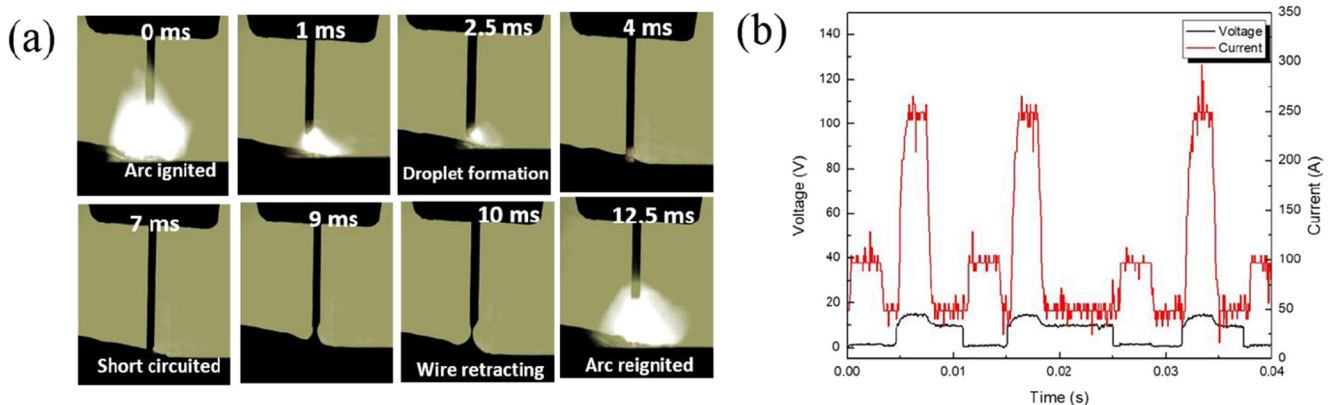
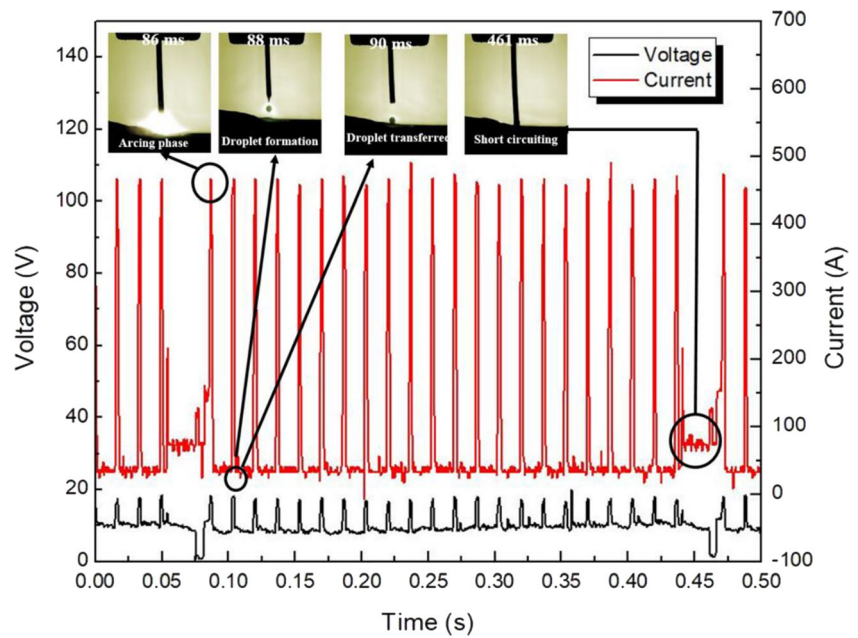


Fig. 4 Droplet transfer behaviour during the short-circuiting process (a) and corresponding current and voltage waveform (b)

Fig. 5 Droplet transfer behaviour during short-circuiting with the pulse process and corresponding current and voltage waveform



arc ignition, and the arcing current was continuously increased up to the peak current of 500 A (I_p). At each peak current, the droplet detached to the weld pool resulting in one droplet transfer per pulse. Arc energy during this deposition was 176 J mm^{-1} for an instantaneous current (I_i) of 85 A.

In both modes of deposition, arc energy was deliberately kept similar (172 and 176 J mm^{-1}) by optimising current-voltage waveforms.

3.2 Microstructural characterisation

Microstructural analysis of the deposited samples was carried out to understand the grain size, grain morphology and possible intermetallic formation as a function of deposition parameters. Preliminary metallography analysis revealed that the deposited samples were found to be free from defects such

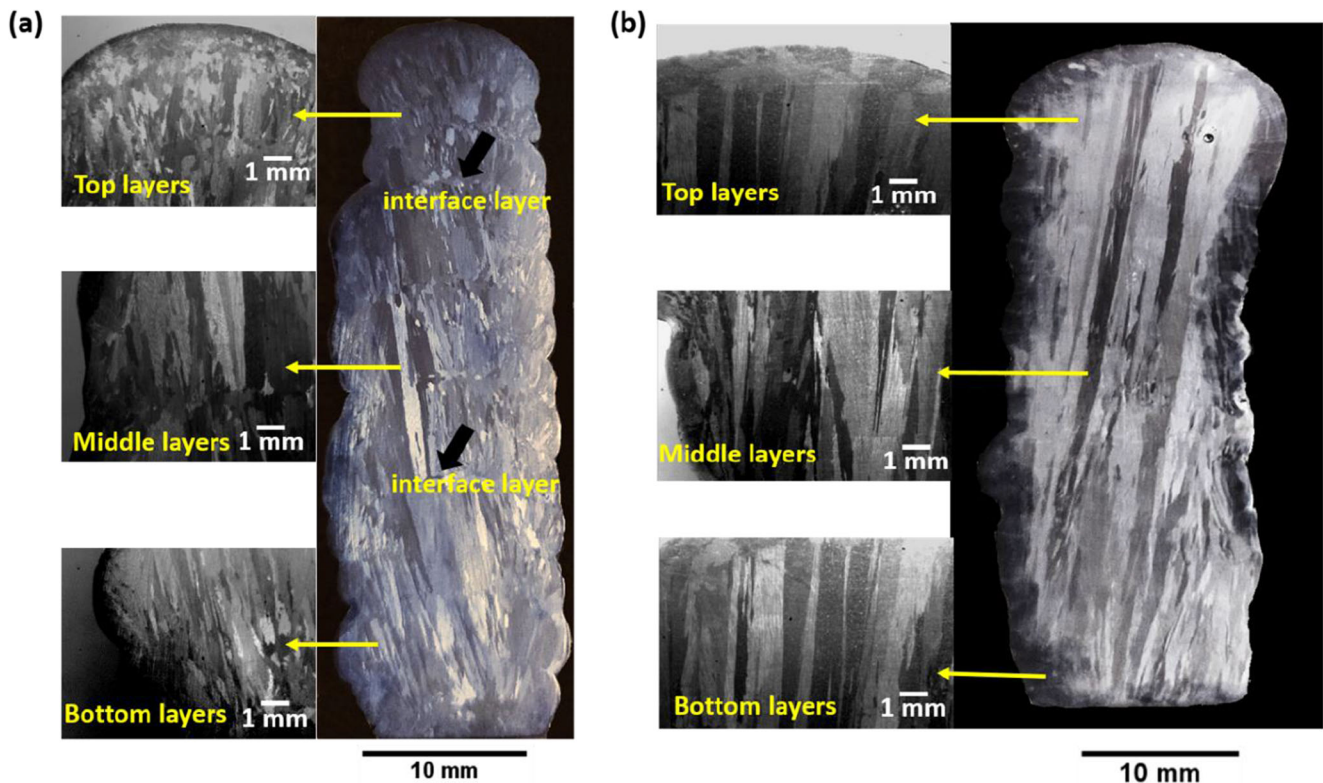


Fig. 6 Macrostructure of Inconel 625 components deposited with short-circuiting (a) and short-circuiting with pulse deposition (b)

as lack of fusion and porosity along the interlayers (Figs. 7 and 8).

Figure 6 shows the macrostructure of Inconel 625 built using short-circuiting mode and short-circuiting with pulse mode of metal transfers. Short-circuiting deposits show columnar grain growth only within the layer, and this growth is found to be discontinued at the layer boundaries. New grains are found to be nucleated at the interface due to heterogeneous nucleation from previously deposited layers (Fig. 6a).

Samples deposited with short-circuiting with pulse mode of metal transfer show a columnar grain growth

across the layers (Fig. 6b). In this mode of deposition, grains are found to be directionally solidified from the substrate surface to the top layers and no clear layer interfaces are observed as in the case of short-circuiting transfer.

The optical microstructures of all the samples deposited with short-circuiting and short-circuiting with the pulse metal transfer are shown in Figs. 7 and 8, respectively. The microstructure of WAAM deposits in the bottom layers comprises cellular grains due to the high cooling rates (Fig. 7a). However, favourable temperature gradient and cooling rates in the middle regions result in columnar grain growth.

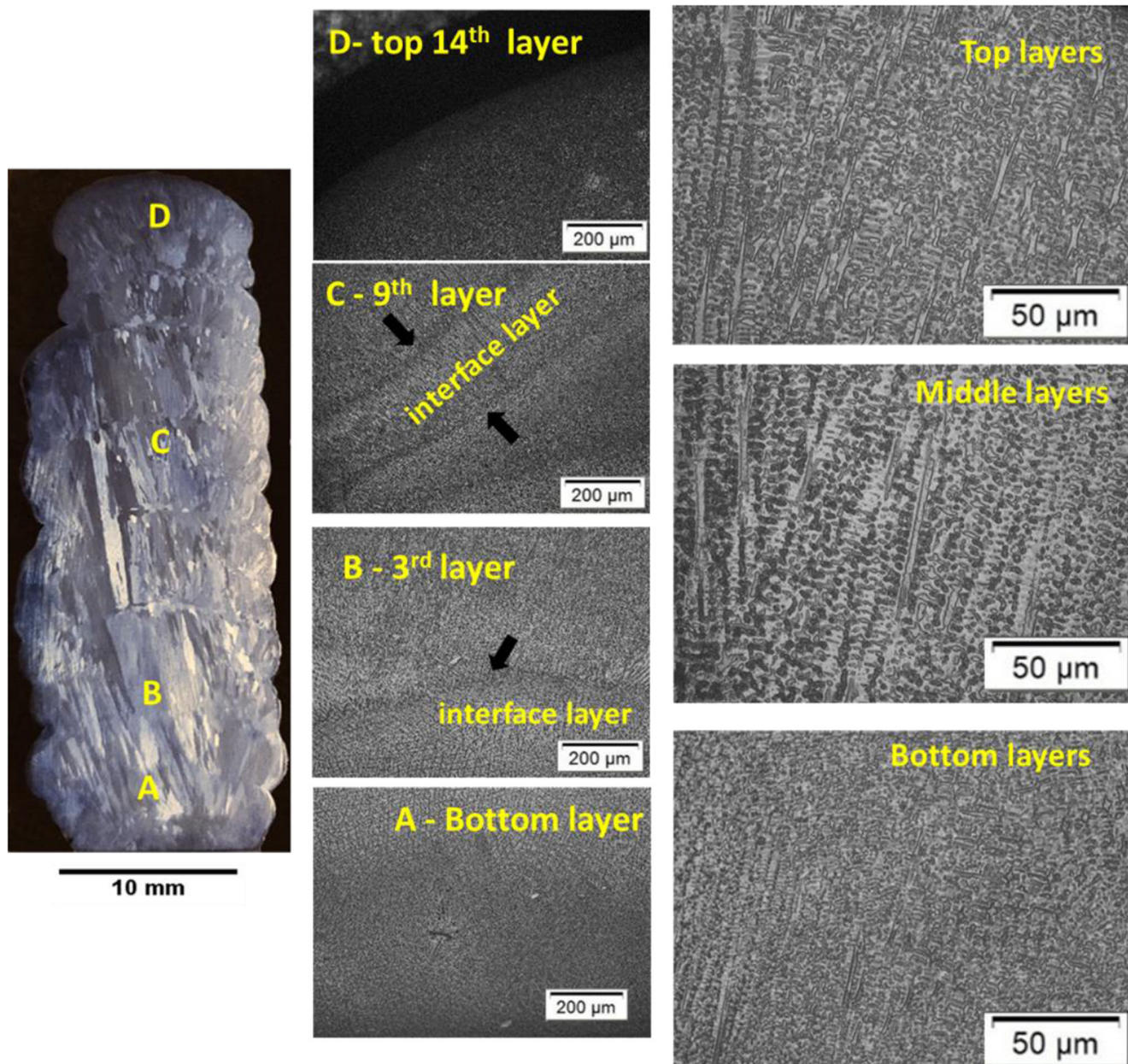


Fig. 7 Microstructure of Inconel 625 component deposited with the short-circuiting mode of metal transfer

The microstructure of the top layers again comprised cellular grains due to the rapid heat transfer to the atmosphere.

It can be clearly seen from Fig. 7 that in short-circuiting mode, grain growth was hindered at the interface boundaries and interfaces were clearly delineated. However, in case of short-circuiting with pulse mode, the microstructure was found to be directionally solidified with a continuous growth solidified grains across the interfaces (Fig. 8). The microstructure of the as-cast sample is shown in Fig. 9. The microstructure was found to be primarily comprising coarse dendritic microstructure.

In order to identify the grain and phase morphology, a scanning electron microscopy (SEM) analysis was carried

out on the WAAM deposits. The SEM analysis indicated that the deposits made by short-circuiting and short-circuiting with pulse transfer (Fig. 10a, b) consisted of two phases, the dark matrix and white bright evenly distributed regions. Energy-dispersive spectroscopy analysis was carried out on these two phases, and results indicated that dark grey was the matrix (FCC phase) and white regions were found to be enriched with Mo and Nb due to the possible segregation of these elements to interdendritic regions during solidification (Fig. 10c).

The SEM microstructure of as-cast Inconel 625 alloy is shown in Fig. 11. The microstructure consisted of a dark matrix with irregular bright white regions. Quantitative analysis was carried out on bright regions by energy-dispersive

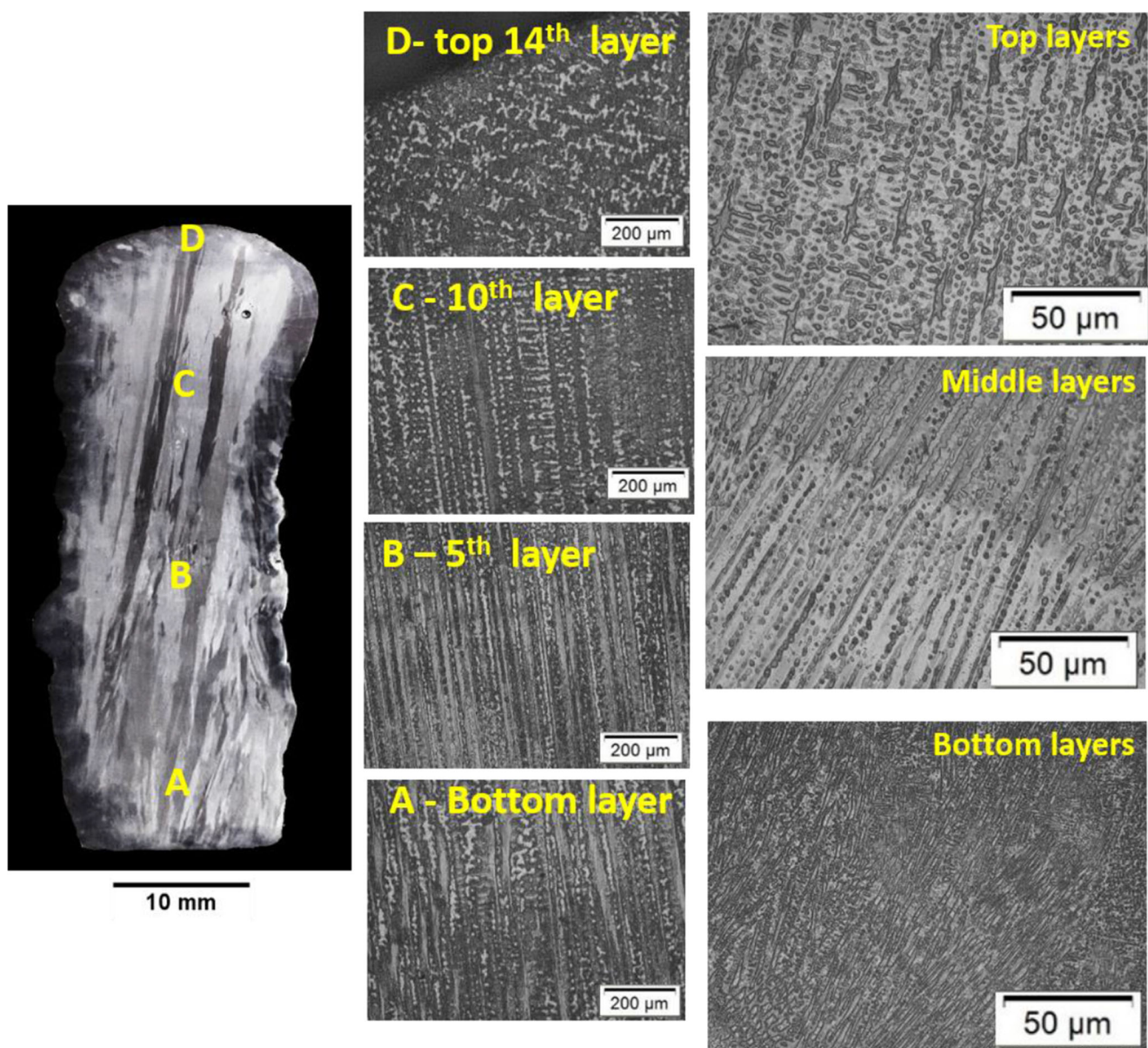


Fig. 8 Microstructure of Inconel 625 component deposited with short-circuiting with pulse mode of metal droplet transfer

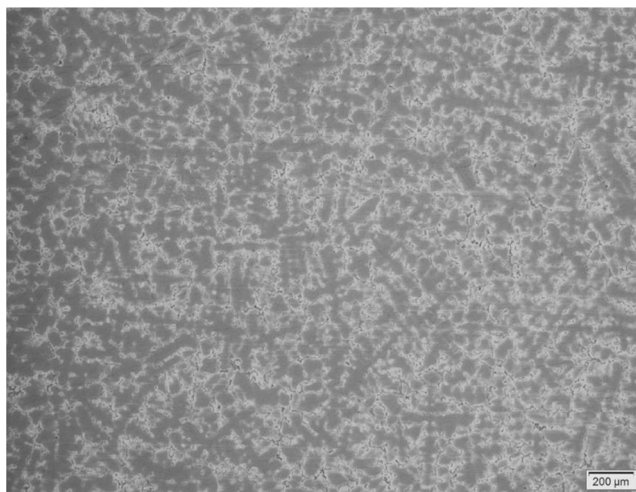


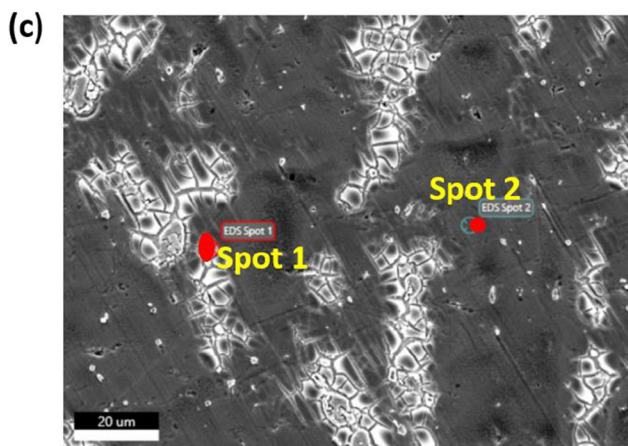
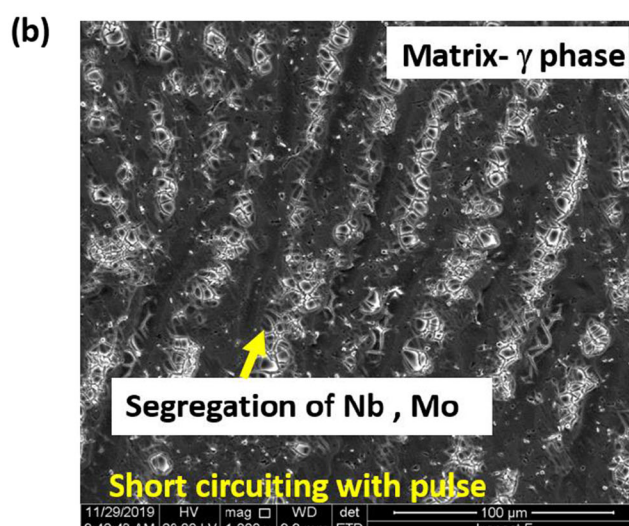
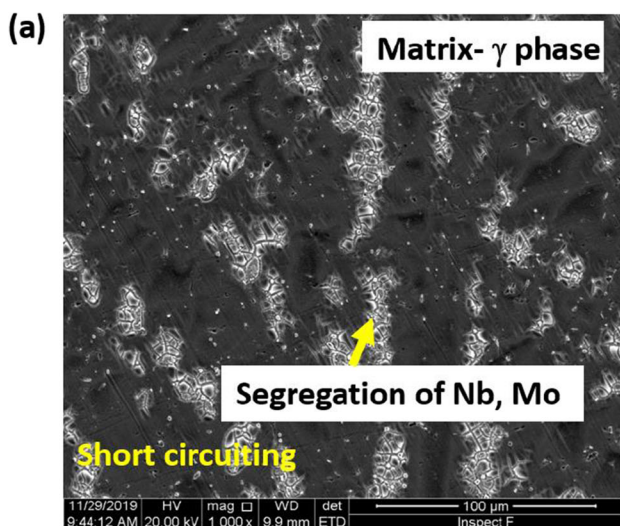
Fig. 9 Microstructure of cast Inconel 625

spectroscopy (EDS), and results showed that the bright white regions were found to be enriched with Nb and Mo as seen in the WAAM deposits.

3.3 Evaluation of mechanical properties

Microhardness measurements were carried out along the transverse direction (*X-Z* plane) of Inconel 625 samples deposited with short-circuiting and short-circuiting with pulse modes. Hardness variation from bottom to top layers along the build (*Z*) direction is shown in Fig. 12. Average hardness was found to be 212 HV_{300g}. The variation in hardness was similar in both samples made using short-circuiting and short-circuiting with pulse modes.

Figure 13 shows the tensile behaviour of Inconel 625 deposits in both transversal (*X-Z* plane) and longitudinal directions (*Y-Z* plane). Tensile testing was carried out with a strain rate of $1 \times 10^{-3} \text{ s}^{-1}$ at room temperature [18]. Yield strength (YS at 0.2% strain) and ultimate tensile stresses (UTS) of deposits along normal and transverse directions are given in Table 3. The tensile strength of short-circuiting and short-circuiting with pulse deposits along the transverse direction (SC-transverse and SCP-transverse, as shown in Fig. 13a) showed higher tensile strength than the as-cast sample.



Spot 1		Spot 2	
Element	Weight %	Element	Weight %
NbL	11.94	NbL	2.33
MoL	16.04	S K	4.03
CrK	21.89	CrK	25.51
FeK	2.32	FeK	1.76
NiK	45.97	NiK	61.44
TaL	1.77	TaL	1.52

Fig. 10 SEM microstructure of Inconel 625 alloy WAAM deposit using short-circuiting (a) and short-circuiting with pulse (b) depositions and image showing the EDS spot analyses (c)

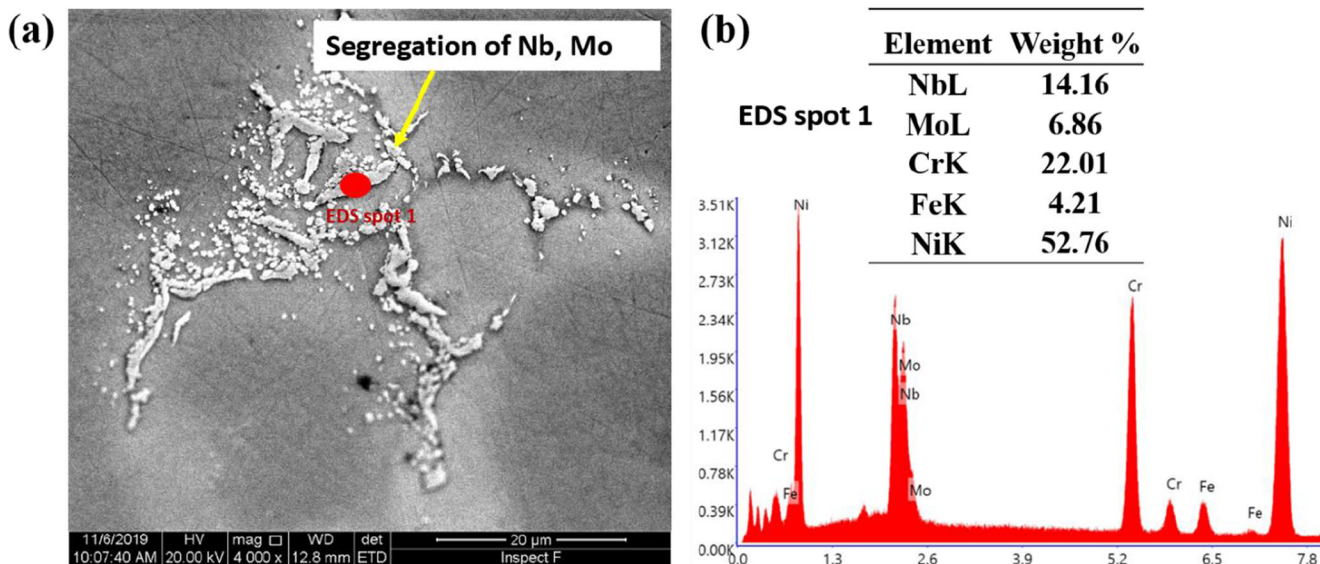


Fig. 11 SEM microstructure of Inconel 625 cast alloy (a) and EDS analysis of microstructure (b)

These samples exhibited higher ultimate strength (UTS) of 580 MPa than samples taken along the longitudinal cross section (SC-longitudinal, SCP-longitudinal), as shown in Fig. 13a. The tensile elongation is more (76%) along the longitudinal direction than transversal direction. It can be clearly seen that the as-cast alloy samples show inferior mechanical properties than WAAM samples (Fig. 13). The fracture surfaces of the samples after tensile testing were analysed using SEM. The fracture surface was found to contain dimples and multivoid coalescences (Fig. 14a–d). The failure morphology clearly indicated that the WAAM samples possessed good strength with excellent ductility, required to meet in-service loading conditions.

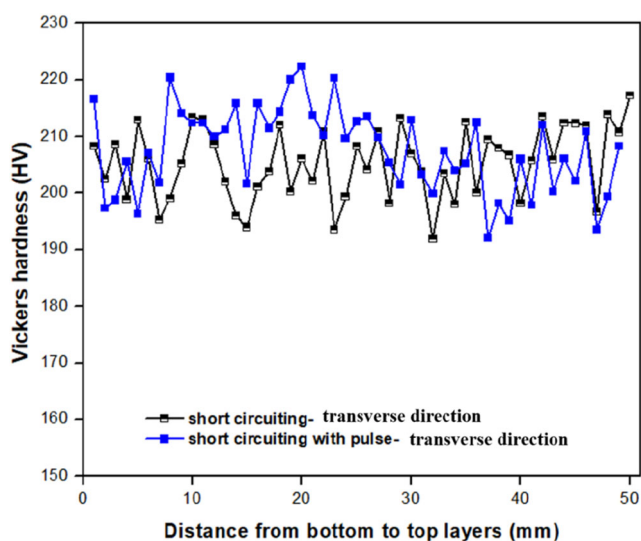


Fig. 12 Hardness distribution of the Inconel 625 WAAM deposits from bottom to top layers

3.4 Electrochemical corrosion behaviour of Inconel 625

The corrosion behaviour of WAAM deposits was analysed by potentiodynamic polarisation and electrochemical impedance spectroscopy analyses. In order to identify the stable electrochemical conditions of the electrolytes, open-circuit potential measurements were carried out. The open-circuit potential (OCP) was measured for all the samples. The OCP was found to be more than 10 mV which denoted that the used electrolyte was always in stable condition.

3.4.1 Potentiodynamic polarisation test

The potentiodynamic polarisation behaviour of short-circuiting and short-circuiting with pulse deposit at the bottom, middle and top layers and cast samples are shown in Figs. 15 and 16, and results are summarised in Table 4. According to Eq. 3, the corrosion current (I_{corr}) is directly proportional to the corrosion rate. It can be seen that the WAAM samples performed better in polarisation tests as compared to cast samples. In short-circuiting deposits, top layers (SC-TL) show good corrosion resistance as compared to other samples extracted from other regions (SC-BL and SC-ML). Similarly, among samples made using short-circuiting with pulse mode, SCP-TL showed good corrosion resistance behaviour as performance compared to the other two cases (SCP-BL and SCP-ML). The results of the polarisation tests are summarised in Fig. 17a.

3.4.2 Electrochemical impedance spectroscopy

Electrochemical impedance spectroscopy (EIS) experiments were performed in order to compare the corrosion resistance of WAAM samples with that of as-cast samples. EIS results were

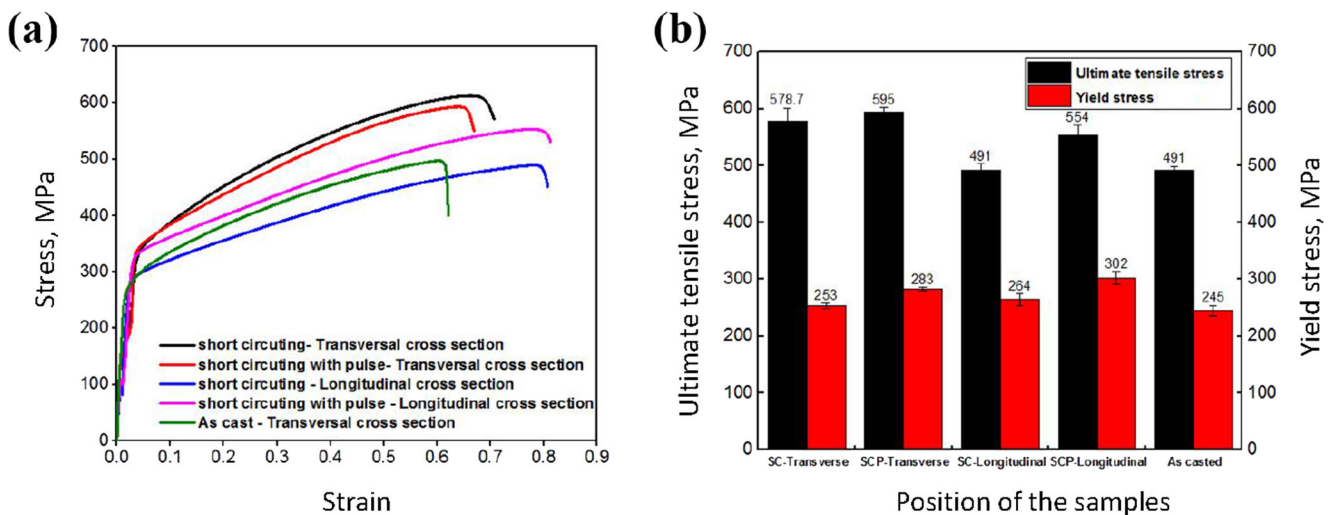


Fig. 13 Stress-strain behaviour during tensile testing of WAAM and conventionally cast samples (a) and comparison of tensile properties as a function of direction with conventionally cast samples (b)

visualised as a Nyquist plot, and the data was fit with a well-known electrical equivalent model (EEC) as shown in Fig. 16. In the equivalent circuit, R_s is the solution resistance, R_f refers to film resistance of the passive film and the constant phase element (CPE) represents film capacitance (see inserts in Fig. 16) [19]. The corrosion resistance of the samples was calculated using the EEC and summarised in Table 5. It can be seen that the WAAM samples performed better in EIS tests as compared to cast samples. In short-circuiting deposits, top layers (SC-TL) show good corrosion film resistance as compared to other samples extracted from other regions (SC-BL and SC-ML). Similarly, among samples made using short-circuiting with pulse mode, SCP-TL showed good corrosion film resistance behaviour as compared to the other two cases (SCP-BL and SCP-ML). The results of the EIS analysis are summarised in Fig. 17b. It can be clearly seen that samples made by short-circuiting with pulse mode deposition possess improved corrosion resistance than short-circuiting and as-cast samples.

4 Discussions

Wire arc additive manufacturing is considered suitable to build large metallic parts due to high deposition rates, process

efficiency and low investment cost. Due to low heat input and negligible amount of spatter in deposition, the controlled dip short-circuiting GMAW-based WAAM process is attractive to build metallic components. In this work, Inconel 625 alloy components are deposited by the GMAW-based WAAM process. Depositions are made by short-circuiting and short-circuiting with pulse mode of droplet transfer using a commercial cold metal transfer gas metal arc welding (CMT-GMAW) power source. It was found from this work that depositing Inconel 625 in short-circuiting and short-circuiting with pulse mode of droplet transfer mode resulted in negligible amount of spatter on deposits. Short-circuiting and short-circuiting with pulse transfer resulted in a stable liquid metal transfer behaviour (Fig. 4 and Fig. 5) during deposition with arc energies of 172 J mm^{-1} and 176 J mm^{-1} , respectively

The macro- and microstructural constituents of the WAAM deposits were thoroughly analysed from the top to bottom layers. The macrostructure of samples deposited with short-circuiting and short-circuiting with pulse mode is given in Fig. 6. The deposits made using both short-circuiting and short-circuiting with pulse transfer showed columnar grain growth. However, the grain growth was found to get discontinued at each layer interface in the short-circuiting mode due to the increased heterogeneous nucleation events on the previously

Table 3 Tensile properties of Inconel 625 samples made by WAAM and conventionally cast sample

Mode droplet transfer	Ultimate tensile strength (MPa)	Yield stress (MPa)	Tensile elongation (%)
Short-circuiting—transversal cross section	578 ± 22	253 ± 5	64.6 ± 4
Short-circuiting with pulse—transversal cross section	595 ± 8	282 ± 2	65.6 ± 4
Short-circuiting—longitudinal cross section	491 ± 12	264 ± 11	76.3 ± 4
Short-circuiting with pulse—longitudinal cross section	554 ± 17	302 ± 12	75.4 ± 5
As-cast sample	491 ± 8	245 ± 9	61 ± 3

deposited layers (Fig. 6a). It was shown that controlled dip short-circuiting transfer led to the promotion of heterogeneous surface nucleation [3]. It can be seen here that this mode of metal transfer hindered the directionally solidified columnar grain growth across the layers [3, 20, 21]. In short-circuiting mode, bottom and top layers contained cellular microstructure due to rapid heat dissipation through the substrate and atmosphere (Fig. 7 at A and D regions) whereas middle layers (3rd to 9th layers) showed columnar grain growth (Fig. 7 at B and C regions).

In the case of short-circuiting with pulse mode deposition, a large number of elongated dendrites have grown across the deposited layers and oriented almost perpendicular to the

substrate in the z -direction (heat-extracted direction). Favourable temperature gradients induced by the super heating of the melt pool by the current pulsing and epitaxial growth from the substrate led to the columnar growth [3, 22]. This grain growth was found to continue across the layer interfaces, and clear evidence of directional solidification was seen from metallography analysis (Fig. 6b).

The microstructure of samples deposited with short-circuiting with pulse mode of transfer contained only directionally solidified grains, growing across the layer interfaces (bottom to top layers). This directionally solidified microstructure was found to be similar to the microstructure produced in conventionally cast nickel-based alloy under

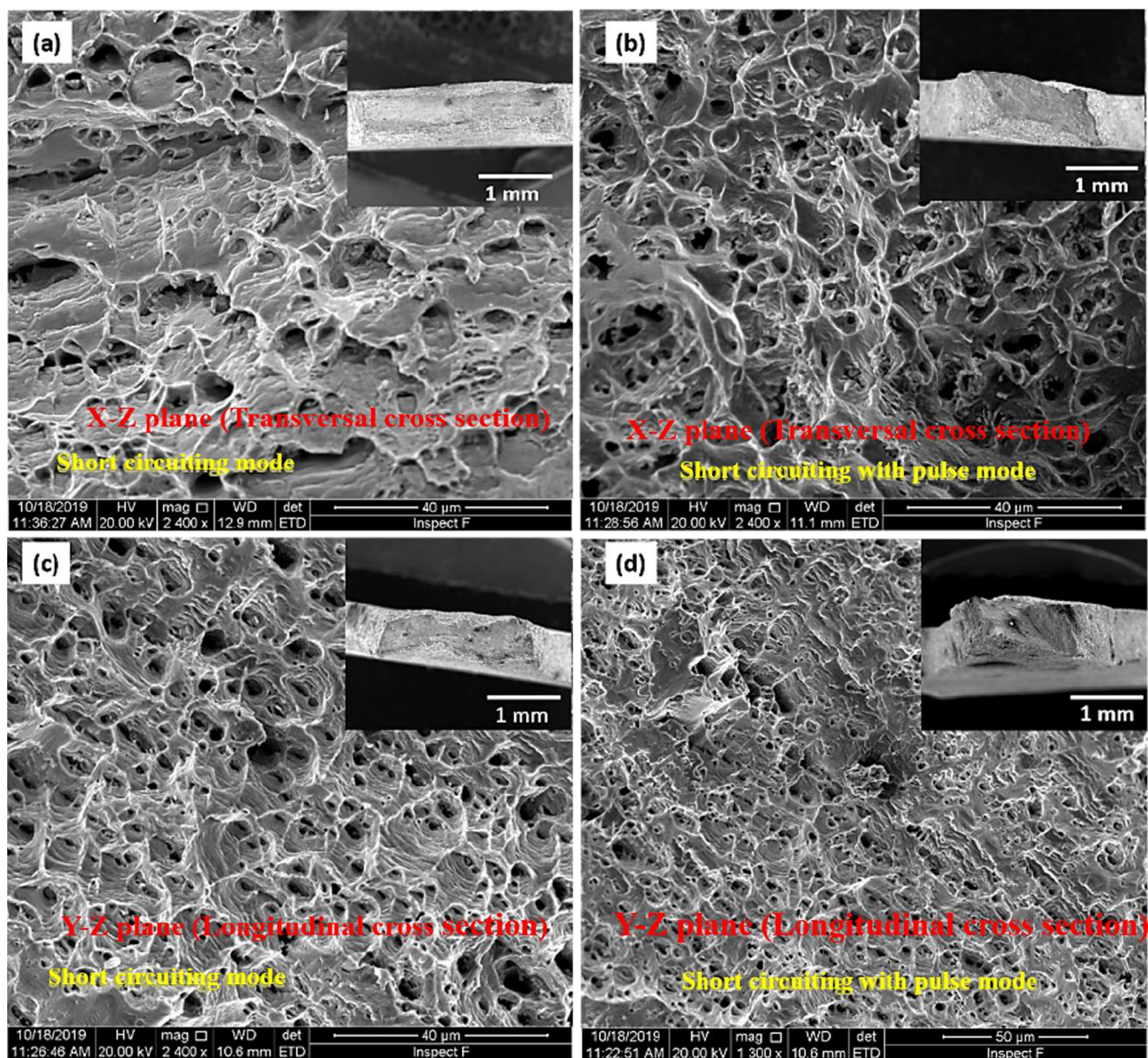


Fig. 14 Tensile fracture surface of WAAM samples deposited with short-circuiting and short-circuiting with pulse, along the transversal cross section (a, b) and along the longitudinal cross section (c, d)

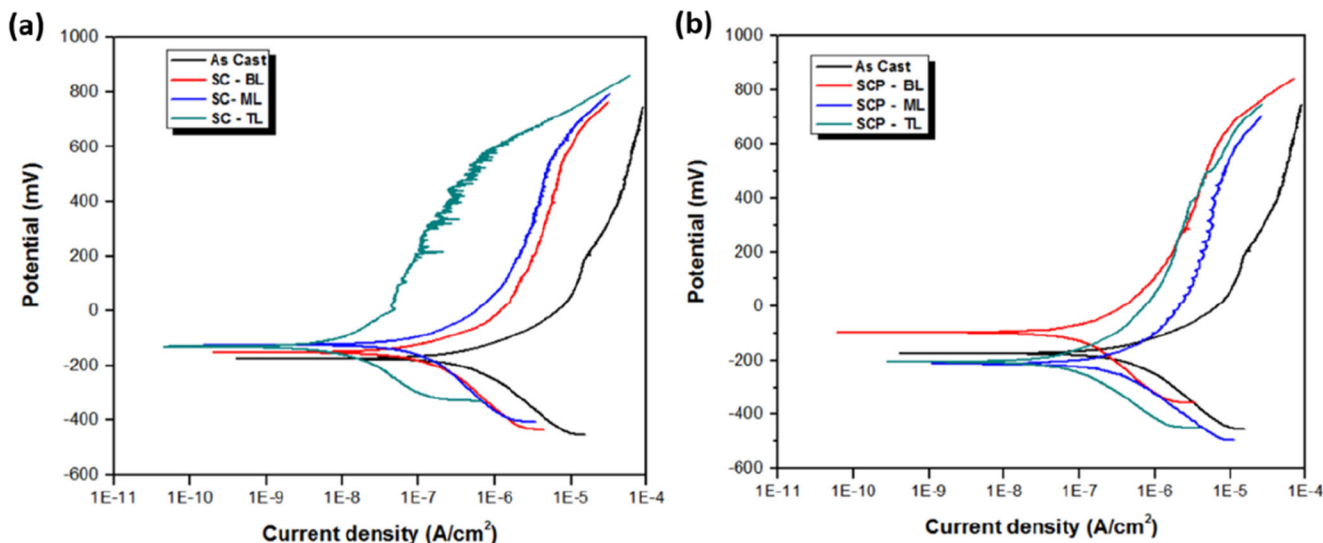


Fig. 15 Potentiodynamic polarisation behaviour of the WAAM Inconel 625 alloy deposits made by short-circuiting (a) and short-circuiting with pulse transfer (b). The polarisation behaviour of the cast sample is shown in both figures as a reference

controlled solidification conditions to promote directional solidification [23]. It is shown here that short circuiting with pulse mode of transfer can produce directionally solidified microstructure without any additional controlled experimental variables. It is also well known that current pulsing leads to an increase in surface temperature of the melt pool [24]. This superheating of the melt pool surface led to the dissolution of heterogenous surface nuclei, thereby promoting directional solidification from the substrate. Moreover, an increase in surface temperature results in steep temperature gradients owing to a combination of convective heat transfer resulting from arc pressure and conduction by substrate/built layers which promote directional solidification along the heat extraction

direction [25]. The microstructure at top layers of the deposit showed cellular dendritic growth (14th layer) due to rapid heat dissipation from the atmosphere and the highest thermal gradient. As compared to the WAAM deposits, the microstructure of as-cast alloy contained coarse columnar grain growth, as shown in Fig. 9.

The SEM analysed indicated that the microstructure of deposits made by short-circuiting, short-circuiting with pulse transfer (Fig. 10) and cast sample (Fig. 11) contained a matrix (FCC phase) and segregation of Mo and Nb elements at the solidification grain boundaries. In general, the segregation of these alloying elements leads to the formation of detrimental intermetallic phases under conductive cooling rates [22].

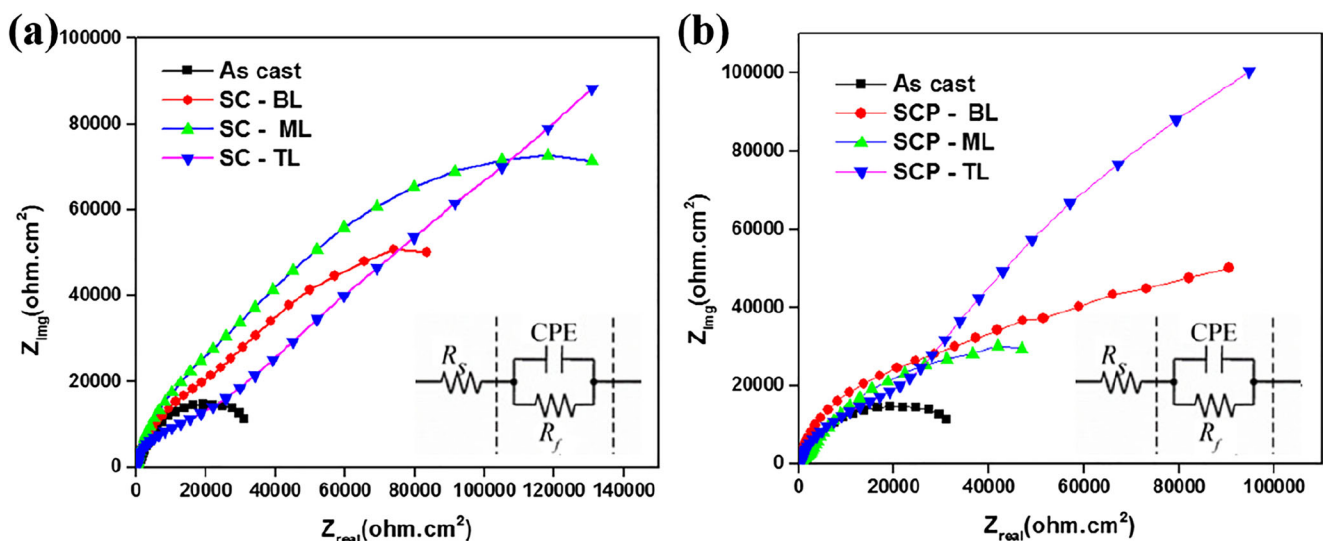


Fig. 16 Nyquist plots of WAAM Inconel 625 samples. Short-circuiting versus conventionally cast (a) and short-circuiting with pulse versus conventionally cast (b)

Table 4 Potentiodynamic polarisation data of samples

Samples	E_{corr} (mV)	I_{corr} ($\mu\text{A}/\text{cm}^2$)	Corrosion rate (mm/year)
As cast	– 175	0.65	0.00645
Short-circuiting bottom 4 layers (SC-BL)	– 152	0.19	0.00192
Short-circuiting middle 4 layers (SC-ML)	– 125	0.21	0.00213
Short-circuiting top 4 layers (SC-TL)	– 224	0.13	0.00128
Short-circuiting with pulse bottom 4 layers (SCP-BL)	– 96	0.336	0.00424
Short-circuiting with pulse middle 4 layers (SCP-ML)	– 213	0.43	0.0045
Short-circuiting with pulse top 4 layers (SCP-TL)	– 249	0.135	0.001425

However, in the samples analysed in this work, there was no clear evidence on the presence of intermetallic phases found from the microstructural analysis. Moreover, the mechanical properties of the WAAM samples were found to be better than those of the as-cast samples. This indicated that the samples contained primarily solid solution strengthened matrix with segregation of alloying elements at the grain boundaries.

Microhardness measurements were carried out on the (X - Z plane) Inconel 625 samples deposited with short-circuiting and short-circuiting with pulse transfer process. The average hardness of WAAM deposits was found to be 212 HV at 300 g load, from bottom to top layers, as shown in Fig. 12. The results of tensile testing indicated that yield stress (YS), ultimate tensile stress (UTS) and tensile elongation of WAAM deposits were higher than for as-cast alloy (Fig. 13). Short-circuiting and short-circuiting with pulse samples along the transverse (X - Z) direction showed higher UTS as compared to the longitudinal (Y - Z) direction (Fig. 13b). Tensile elongation of WAAM deposits was found to be higher along the longitudinal direction (76%) than transversal direction (65%). Results indicated that the samples extracted along the transversal cross section (X - Z plane, as shown in Fig. 14a, b)

showed better mechanical properties and fracture surfaces exhibiting a combination of dimples and cleavage planes. The fractography of samples extracted along the longitudinal directions (Fig. 14c, d) contained dimples of varying sizes, resulting from the improved ductility as compared to the other samples. Samples produced by both modes of droplet transfer showed better mechanical properties than the as-cast sample which contained coarse dendritic microstructures.

The electrochemical experiments were carried out on WAAM and as-cast samples. The kinetics of the corrosion process can be described by the change in corrosion current density (I_{corr}). The I_{corr} values of short-circuiting samples was 0.13, 0.21 and 0.19 $\mu\text{A cm}^{-2}$, in sample locations SC-TL, SC-ML and SC-BL, respectively. These I_{corr} values were found to be lower than that of the as-cast samples (0.65 $\mu\text{A cm}^{-2}$). Similarly, the top layers of short-circuiting with pulse deposit (SCP-TL) showed low (0.135 $\mu\text{A cm}^{-2}$) I_{corr} values as compared to SCP-ML and SCP-BL (Fig. 17a). EIS analysis also confirmed the results of polarisation measurements. The solution resistance (R_s) of WAAM and as-cast samples in a 0.1 M % NaCl solution were similar. However, significant differences in passive film resistance (R_f) were observed, while

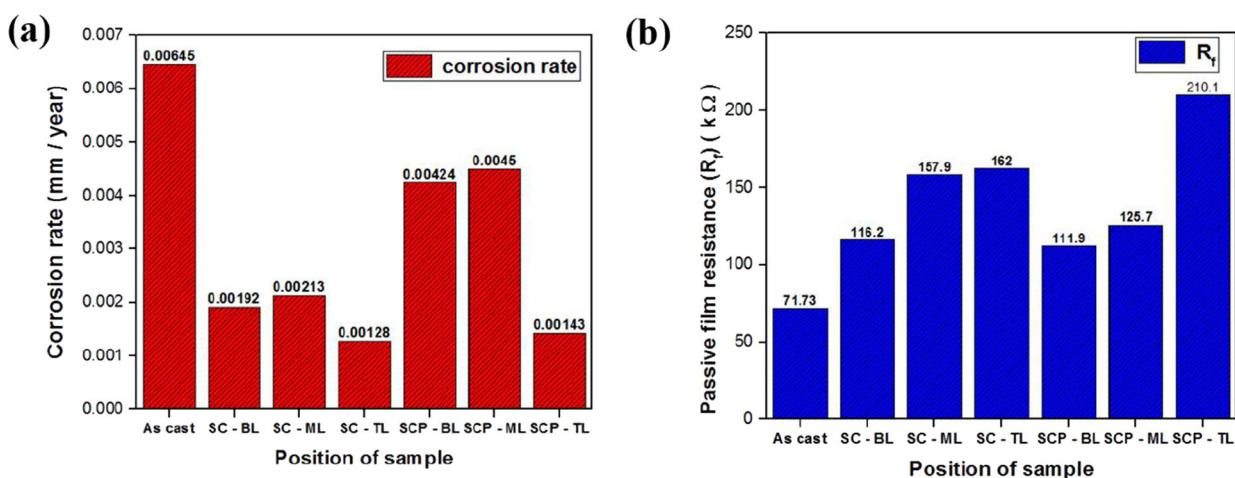


Fig. 17 Corrosion behaviour of WAAM samples at various locations, corrosion rate (a) and passive film resistance (b) (note: refer to Fig. 3 for sample location details)

Table 5 Corrosion data measured using electrochemical impedance spectroscopy

Samples	R_s (Ω)	R_f (k Ω)	Q_f (S.sec ⁿ cm ⁻²)	n
As cast	242.8	71.73	78.41×10^{-6}	0.671
Short-circuiting bottom 4 layers (SC-BL)	261.7	116.2	20.08×10^{-6}	0.800
Short-circuiting middle 4 layers (SC-ML)	277.7	157.9	16.52×10^{-6}	0.813
Short-circuiting top 4 layers (SC-TL)	268.2	162	32.05×10^{-6}	0.707
Short-circuiting with pulse bottom 4 layers (SCP-BL)	271.1	111.9	20.78×10^{-6}	0.870
Short-circuiting with pulse middle 4 layers (SCP-ML)	263.7	125.7	60.37×10^{-6}	0.688
Short-circuiting with pulse top 4 layers (SCP-TL)	285.3	210.1	24.17×10^{-6}	0.724

SC-TL and SCP-TL samples showed (Fig. 17b) the highest value of R_f (162 k Ω , 210 k Ω), indicating best corrosion resistance at these locations. SC-ML, SC-BL, SCP-BML and SCP-BL samples exhibit a lower average R_f value (116.2 k Ω , 157.9 k Ω , 111.9 k Ω and 125.7 k Ω , respectively), but distinctively higher than that of as-cast samples (71.73 k Ω). In general, a high R_f value of passive film implies good corrosion resistance. Based on these results, it can be concluded that WAAM deposits possess better corrosion resistance than as-cast Inconel 625. Moreover, the corrosion resistance of samples produced by short circuiting with pulse mode of transfer showed improved corrosion resistance than all other samples, resulting from the directionally solidified columnar grains containing microstructures.

5 Conclusions

In the present study, the effect of droplet transfer on microstructure mechanical properties and corrosion behaviour of Inconel 625 components is investigated. The following conclusions can be drawn based on the obtained results:

1. Inconel 625 alloy samples were successfully fabricated by using a GMAW-based process without defects and lack of fusion at the interlayers. The samples produced by short-circuiting transfer showed discontinuous grain growth across the interface. However, a clear directionally solidified microstructure was contained by short-circuiting with pulsed mode of droplet transfer.
2. The microstructure of WAAM samples consisted of a γ -FCC matrix with segregation Nb and Mo elements in the interdendritic regions and grain boundaries.
3. Samples produced by WAAM exhibited better tensile strengths and elongation than as-cast samples, indicating the absence of any detrimental intermetallic phases.
4. Samples made using short-circuiting with pulsing transfer showed good tensile elongation and excellent corrosion resistance than other samples due to the stabilisation of directionally solidified columnar grain structure.

5. The potentiodynamic polarisation and electrochemical impedance spectroscopy analysis confirmed that WAAM samples exhibited better corrosion properties than cast samples.

References

1. DebRoy T, Wei H, Zuback J, Mukherjee T, Elmer J, Milewski J, Beese AM, Wilson-Heid A, De A, Zhang W (2018) Additive manufacturing of metallic components – Process, structure and properties. *Prog Mater Sci* 92:112–224
2. Williams SW, Martina F, Addison AC, Ding J, Pardo G, Colegrove P (2016) Wire + Arc Additive Manufacturing. *Mater Sci Technol* 32(7):641–647
3. Baby J, Amirthalingam M (2020) Microstructural development during wire arc additive manufacturing of copper-based components. *Weld World* 64(2):395–405
4. Martina F, Mehnen J, Williams SW, Colegrove P, Wang F (2012) Investigation of the benefits of plasma deposition for the additive layer manufacture of Ti–6Al–4V. *J Mater Process Technol* 212(6):1377–1386
5. Shankar V, Rao KBS, Mannan S (2001) Microstructure and mechanical properties of Inconel 625 superalloy. *J Nucl Mater* 288(2–3):222–232
6. Paul CP, Ganesh P, Mishra S, Bhargava P, Negi J, Nath A (2007) Investigating laser rapid manufacturing for Inconel-625 components. *Opt Laser Technol* 39(4):800–805
7. Frazier WE (2014) *J Mater Eng Perform* 23(6):1917
8. Thivillon L, Bertrand P, Laget B, Smurov I (2009) Potential of direct metal deposition technology for manufacturing thick functionally graded coatings and parts for reactors components. *J Nucl Mater* 385(2):236–241
9. Xu F, Lv Y, Liu Y, Shu F, He P, Xu B (2013) Microstructural Evolution and Mechanical Properties of Inconel 625 Alloy during Pulsed Plasma Arc Deposition Process. *J Mater Sci Technol* 29(5):480–488
10. Cheepu M, Lee CI, Cho SM (2020) *Transactions of the Indian Institute of Metals* pp. 1–5
11. Wang J, Sun Q, Wang H, Liu J, Feng J (2016) Effect of location on microstructure and mechanical properties of additive layer manufactured Inconel 625 using gas tungsten arc welding. *Mater Sci Eng A* 676:395–405
12. Tanvir A, Ahsan MR, Ji C, Hawkins W, Bates B, Kim DB (2019) Heat treatment effects on Inconel 625 components fabricated by wire + arc additive manufacturing (WAAM)—part 1: microstructural characterization. *Int J Adv Manuf Technol* 103(9–12):3785–3798

13. Yangfan W, Xizhang C, Chuanchu S (2019) Surface and Coatings Technology
14. Cabrini M, Lorenzi S, Testa C, Pastore T, Brevi F, Biamino S, Fino P, Manfredi D, Marchese G, Calignano F, Scenini F (2019) Evaluation of Corrosion Resistance of Alloy 625 Obtained by Laser Powder Bed Fusion. *J Electrochem Soc* 166(11):C3399–C3408
15. Wang Y, Chen X (2019) Investigation on the microstructure and corrosion properties of Inconel 625 alloy fabricated by wire arc additive manufacturing. *Mater Res Express* 6(10):106568
16. Guo Q, Li Y, Qian J, Yu H, Chen C (2017) *Int J Electrochem Sci* 12(10):8929
17. Norrish J (2006) *Advanced welding processes*. Elsevier
18. Fontana MG (2005) *Corrosion engineering*. Tata McGraw-Hill Education
19. Fonseca C, Barbosa MA (2001) Corrosion behaviour of titanium in biofluids containing H₂O₂ studied by electrochemical impedance spectroscopy. *Corros Sci* 43(3):547–559
20. Ravi G, Murugan N, Arulmani R (2020) Microstructure and mechanical properties of Inconel-625 slab component fabricated by wire arc additive manufacturing. *Mater Sci Technol* 36(16):1785–1795
21. Jiang Q, Zhang P, Yu Z, Shi H, Li S, Wu D, Yan H, Ye X, Chen J (2020) Microstructure and mechanical properties of thick-walled Inconel 625 alloy manufactured by wire arc additive manufacture with different torch paths. *Adv Eng Mater*. <https://doi.org/10.1002/adem.202000728>
22. Lippold JC, Kiser SD, DuPont JN (2011) *Welding metallurgy and weldability of nickel-base alloys*. John Wiley & Sons, Hoboken, NJ
23. Versnyder FI, Shank ME (1970) The development of columnar grain and single crystal high temperature materials through directional solidification. *Mater Sci Eng* 6.4:213–247
24. Saedi HR, Unkel W (1988) Arc and weld pool behavior for pulsed current GTAW. *Weld J* 67(11):247
25. Knapp GL et al (2019) Experiments and simulations on solidification microstructure for Inconel 718 in powder bed fusion electron beam additive manufacturing. *Addit Manuf* 25:511–521

Publisher's note Springer Nature remains neutral with regard to jurisdictional claims in published maps and institutional affiliations.